PERGAMON

International Journal of Heat and Mass Transfer 45 (2002) 1211–1227

International Journal of HEAT and MASS TRANSFER

www.elsevier.com/locate/ijhmt

# Stationary transverse rolls and U-rolls in limiting low Reynolds number mixed convective air flow near the convective threshold in a horizontal flat duct

T.C. Cheng, J.T. Lir, T.F. Lin *

*Department of Mechanical Engineering, National Chiao Tung University, 1001 Ta Hsueh Road, Hsinchu 30010, Taiwan*

Received 29 June 2000; received in revised form 6 July 2001

**Abstract**

Combined experimental flow visualization and temperature measurement are carried out in the present study to explore the buoyancy driven vortex flow patterns in a limiting low Reynolds number mixed convective air flow through a bottom heated horizontal flat duct. In Particular, attention is paid to the flow approaching the natural convection limit ($Re = 0$) for $Re = 1.0$ and 2.0 with the Rayleigh number near the critical level for the onset of convection for $1200 \leqslant Ra \leqslant 4000$. Results from the flow visualization have revealed two unfamiliar vortex flow patterns which were not seen in our earlier study [Int. J. Heat Mass Transfer 44 (4) (2001) 705]. One is characterized by the stable stationary transverse rolls in the duct entry and stable longitudinal rolls in the downstream. Another is in the form of U-rolls. The relations of these two patterns with those reported in the literature from analytical, numerical and experimental studies are discussed. Moreover, stable longitudinal rolls along with nonperiodic traversing waves, and mixed longitudinal and transverse rolls as well as irregular cells which appear in the higher Reynolds number for $3.0 \leqslant Re \leqslant 5.0$ are also noted here. The temporal and spatial characteristics of the unfamiliar vortex flows are inspected in detail. In addition, the flow formation processes leading to the two unfamiliar vortex flow structures are also examined carefully. During the flow formation we noted merging of longitudinal and transverse rolls to form U-rolls, splitting of rolls into cells and the reverse process of cell integration into rolls, aside from the generation of the longitudinal and transverse rolls. Finally, a flow regime map is provided to delineate various vortex flow structures observed in this study and in the previous study (cf. the above-mentioned reference) driven by the slightly supercritical and subcritical buoyancies for $1.0 \leqslant Re \leqslant 5.0$. 

## 1. Introduction

Buoyancy driven vortex flow structure is known to be significantly affected by the Reynolds and Rayleigh numbers in a mixed convective flow through a bottom heated horizontal flat duct, as evident from various experimental studies [1–7]. Depending on the level of the Reynolds number, longitudinal, transverse or mixed vortex rolls are frequently induced by the supercritical buoyancy. Recently, we [8] experimentally revealed two additional vortex flow patterns at slightly supercritical and subcritical Rayleigh numbers for the relatively low Reynolds numbers with $Re = 3.0$, 4.0 and 5.0. More specifically, we observed a vortex flow characterized by steady longitudinal rolls near the duct sides along with nonperiodic moving transverse waves in the duct core. Another vortex flow is in the form of steady longitudinal rolls in the sidewall region, time periodic moving transverse rolls in the entry half of the duct core, and irregular cells in the exit half of the duct core. Besides, we also noted that even at these low Reynolds numbers steady longitudinal vortex flow is induced at slightly subcritical buoyancy. It is of interest to unveil the possible presence of the additional vortex flow structures for even lower Reynolds numbers for $Re$ approaching zero. The understanding of this limiting low Reynolds number mixed convective vortex flow of gas is especially

* Corresponding author. Tel.: +886-35-712121; fax: +886-35-720634.

*E-mail address:* t7217@cc.nctu.edu.tw (T.F. Lin).

0017-9310/02/$ - see front matter 
PII: S0017-9310(01)00229-0

**Nomenclature**

| | |
|---|---|
| $A$ | aspect ratio ($b/d$) |
| $b, d$ | channel width and height |
| $g$ | gravitational acceleration |
| $Gr$ | Grashof number ($\beta g d^3(T_h - T_c)/\nu^2$) |
| $Pr$ | Prandtl number ($\nu/\alpha$) |
| $Ra$ | Rayleigh number ($\beta g d^3(T_h - T_c)/\alpha\nu$) |
| $Ra_c$ | critical Rayleigh number corresponding to the onset of convection for an infinite layer |
| $Re$ | Reynolds number ($W_m d/\nu$) |
| $t$ | time (s) |
| $t_p$ | oscillation period (s) |
| $T$ | temperature |
| $T_c, T_h$ | temperatures of the cold and hot plates |
| $T_m$ | mean temperature ($(T_h + T_c)/2$) |
| $W, W_m$ | velocity and average velocity components in $z$ direction |
| $x, y, z$ | dimensionless Cartesian coordinates scaled with $d$ |
| $\alpha$ | thermal diffusivity |
| $\beta$ | thermal expansion coefficient |
| $\theta$ | dimensionless temperature ($(T - T_m)/(T_h - T_c)$) |
| $\nu$ | kinematic viscosity |

important in the growth of single crystal films from chemical vapor deposition [9].

In a mixed convective flow through a bottom heated horizontal flat duct the onset of the longitudinal vortex flow due to thermal instability was found to occur at the critical Rayleigh number $Ra_c^L \approx 1708$ independent of the Reynolds number of the flow and Prandtl number of the fluid [10–13]. Beyond this critical Rayleigh number, steady longitudinal rolls prevail and the roll diameter is nearly equal to the duct height. The corresponding spanwise temperature distribution has regular sinusoidal shape [10]. Kamotani and Ostrach [11,12] found that the regular sinusoidal temperature distributions were distorted and there were no stable vortex rolls for $Re = 38$ as $Ra > 8000$.

Various vortex structures driven by the buoyancy were delineated by a flow regime map including the flow with no vortex roll, steady and unsteady longitudinal rolls, transverse rolls and unsteady intermittent rolls [1–5]. Moffat and Jensen [14,15] suggested that the buoyancy driven secondary flow structure was very sensitive to the duct aspect ratio. Müller et al. [16–18] solved the simplified modal amplitude equations for a low Reynolds number flow to predict the structures of longitudinal and transverse vortex flows.

The existence of the transverse thermoconvective rolls was proved by Luijkx and Platten [19] at very low Reynolds numbers. The critical Rayleigh number corresponding to the onset of the transverse rolls $Ra_c^T$ was found to be a function of the aspect ratio and Prandtl number, and $Ra_c^T$ increased with the Reynolds number [19,20]. Beyond the critical Rayleigh number $Ra_c^T$, different vortex flow patterns may compete depending on the Reynolds number. Steady and unsteady longitudinal rolls, time-periodic moving transverse rolls, and somewhat irregular snaking rolls were reported from our group [7]. Ouazzani et al. [3–5] refined the flow regime map to include the transverse rolls for air flow.

An interesting vortex flow pattern consisting of transverse rolls in the entry portion of the duct and longitudinal rolls in the downstream which prevailed at relatively low Reynolds numbers was predicted decades ago by a linear stability analysis from Cheng and Wu [21]. The pattern was later confirmed by the experimental flow observation [22] and numerical simulation [16,22–24]. The physical explanation for the appearance of this pattern was provided by Müller et al. [16].

Recently, combined flow visualization and temperature measurement were carried out to explore the mixed convective air flow for $1 \leqslant Re \leqslant 50$ and $1800 \leqslant Ra \leqslant 30{,}000$ by Chang and Lin and their colleagues [6,7]. Their results revealed six vortex flow patterns : (1) stable longitudinal rolls, (2) unstable longitudinal rolls, (3) unstable longitudinal to transverse roll transition, (4) mixed longitudinal/transverse rolls, (5) transverse rolls and (6) irregular rolls. Based on a linear stability analysis, Nicolas et al. [25] suggested that when the Rayleigh number exceeded certain critical value, the instabilities appeared in the form of three-dimensional horseshoe transversal rolls or longitudinal rolls.

A close examination of the above literature reveals that the buoyancy driven vortex flow in a mixed convective gas flow through a flat duct at a limiting low Reynolds number approaching zero remains poorly understood. To complement these early studies, an experiment including detailed flow visualization and temperature measurement is carried out here to investigate the temporal and spatial characteristics of the vortex flow structure for mixed convection of air in a horizontal plane channel at very low Reynolds number for $Re \leqslant 2.0$. Note that at this low Reynolds number the buoyancy-to-inertia ratio $Gr/Re^2$ is still relatively high even for a subcritical buoyancy and it is reasonable to expect the existence of some vortex flow at the subcritical state [8,26]. Thus the Rayleigh number will be varied from 1200 to 4000.

## 2. Experimental apparatus and procedures

The schematic diagram of the test apparatus which is modified slightly from our previous study [6] is shown in Fig. 1. In the following the apparatus is briefly described. More complete details on the experimental system and procedures are given in our recent work [8]. The open-loop mixed convection apparatus consists of three parts: wind tunnel, test section, and measuring bench for the velocity and temperature probes along with the data acquisition system. The test section is a rectangular duct of 240 mm wide and 300 mm long with 15 mm in height between the top cooled and bottom heated plates, providing an aspect ratio of $A = 16$. It should be noted that the duct height is reduced from 20 mm used in the previous study to 15 mm in this study. This narrower gap ($d = 15$ mm) could provide a better

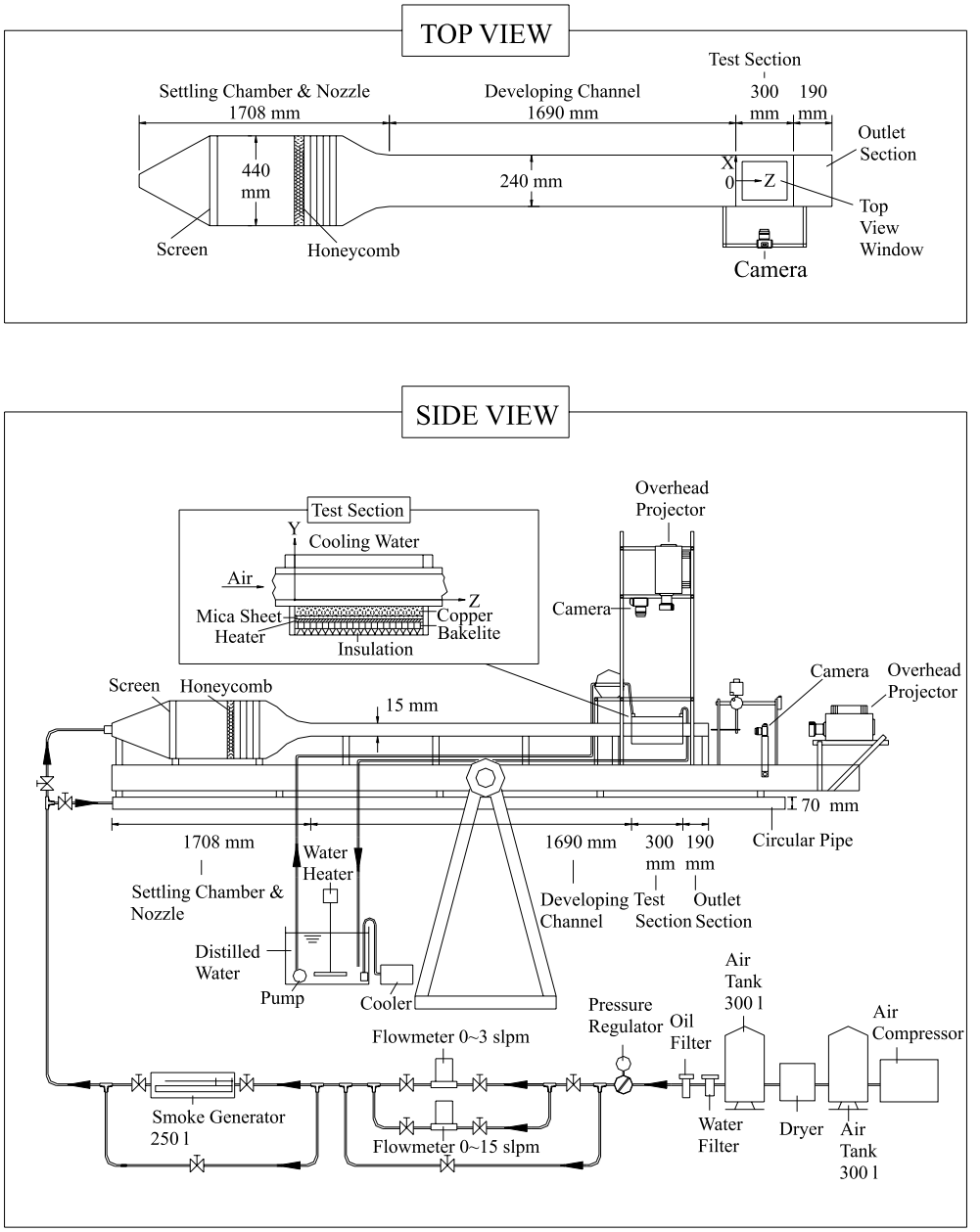


Fig. 1. Schematic of test apparatus and the chosen coordinate system.

control of the temperature difference between the horizontal plates even at very low Rayleigh numbers to be covered in the present study. The bottom plate of the test section is made of a 20-mm-thick, high purity copper plate and is heated by dc power supplies. The top plate of the test section is made of a 3-mm -thick glass plate and a 2-mm-thick plexiglass plate with a gap width of 3 mm. This top plate is reinforced by copper alloy frames to keep it flat. Distilled water is provided from a tank and flows into this gap to cool the upper plate. The working fluid is air which is driven by a 7.5 hp air compressor and is sent into a 300-l and 100 psi high-pressure air tank. The air is first regulated by a pressure regulator and then is passed through a settling chamber, a contraction nozzle, a developing section and finally the test section. The developing section is 1660 mm in length, approximately 110 times of the duct height. This insures the flow being fully developed at the inlet of the test section for $Re \leqslant 50$. An insulated outlet section of 160 mm long is added to the test section to reduce the effects of the disturbances from discharging the flow to the ambient surrounding of the open-loop wind tunnel.

The volume flow rate of air is controlled and measured by two Hasting HFC flow controllers designed especially for low volume flow rates, with accuracy better than 1%. A thermocouple probe, which is an OMEGA (model HYP-O) mini hypodermic extremely small T-type thermocouple (33 gauge) implanted in a 1 in. long stainless steel hypodermic needle, is used to measure the instantaneous temperature of the air flow in the duct.

Flow visualization is performed by injecting smoke tracer into the flow to observe the secondary flow structure. Specifically, the tiny incense smoke is injected into the main flow at some distance ahead of the settling chamber. By using a 1.5–2.5 mm plane light beam of an overhead projector with an adjustable knife edge to illuminate the flow field containing these smoke particles, a sharp contrast could be obtained between the duct walls and the smoke.

Uncertainties in the Rayleigh number, Reynolds number and other independent parameters are calculated according to the standard procedures established by Kline and McClintock [27]. The uncertainties of the thermophysical properties of the air are included in the analysis. The properties of the working fluid (air) are $\alpha = 0.22$ ($\mathrm{cm}^2/\mathrm{s}$), $\beta = 0.0034$ (1/K), $\nu = 0.162$ ($\mathrm{cm}^2/\mathrm{s}$) and $Pr = 0.74$ at 30 °C and 1.0 bar. In addition, the uncertainties of the control unsteadiness and temperature nonuniformity are accounted for in the evaluation of the data uncertainty. The analysis shows that the uncertainties of temperature, volume flow rate, dimensions, Reynolds number and Rayleigh number measurements are estimated to be less than $\pm 0.15$ °C, $\pm 1\%$, $\pm 0.05$ mm, $\pm 2\%$ and $\pm 5\%$, respectively.

## 3. Results and discussion

Selected results from the present study will be presented in the following to illustrate the vortex flow structures in the limiting low Reynolds number mixed convective air flow for $Re \leqslant 2.0$ subjected to the slightly supercritical and subcritical buoyancies for $1200 \leqslant Ra \leqslant 4000$. Particular attention will be paid to some unfamiliar vortex flow patterns induced in the flow. How these vortex flow structures are formed in the flow will be examined in detail.

### 3.1. Vortex flow patterns at long time

To illustrate the vortex flow structures for various Rayleigh numbers at the limiting low Reynolds numbers, the flow photos taken at the midheight of the duct ($y = 1/2$) from the top view at steady or statistically stable state are shown in the following. Firstly, the change of the vortex flow patterns is manifested in Fig. 2 for the Rayleigh number reducing from 4000 to 1200 at $Re = 2.0$. It has been known for some time that regular moving transverse rolls are normally formed in the flow at very low $Re$ and high $Gr/Re^2$ [3–6,19,24]. This transverse vortex flow pattern can be seen for the Rayleigh number of 2500 (Fig. 2(c)). Note that at this $Ra$ the buoyancy-to-inertia ratio is so large that the moving transverse rolls are repeatedly induced at the duct inlet and are pushed slowly forward by the forced main flow. Raising the Rayleigh number from 2500 to 3000 causes the transverse rolls to grow in spanwise dimension and in strength. It is noted that the induced transverse rolls become somewhat bent and can merge with the neighbor rolls. Thus the vortex rolls are distorted to a certain degree and become unstable as traveling downstream (Fig. 2(b)). For a higher $Ra$ of 4000 the distortion in the transverse rolls is more significant especially in the exit region of the duct (Fig. 2(a)). It is also noted that some irregular vortex flow in the form of connecting recirculating vortices is induced along the duct sides at the lower buoyancy with $Ra = 2500$ (Fig. 2(c)). For the lower $Ra$ of 2000 the transverse rolls are weaker and do not extend to the duct sides. Instead, the longitudinal rolls are induced near the side walls of the duct. Besides, the transverse rolls disintegrate into a number of irregular cells as they move to the exit half of the duct. Thus, at $Ra = 2000$ a mixed vortex flow including the longitudinal rolls near the duct sides, transverse rolls in the upstream core region and irregular cells in the downstream core region is induced in the duct (Fig. 2(d)). At an even lower $Ra$ of 1750 the transverse rolls and irregular cells completely disappear in the duct core and

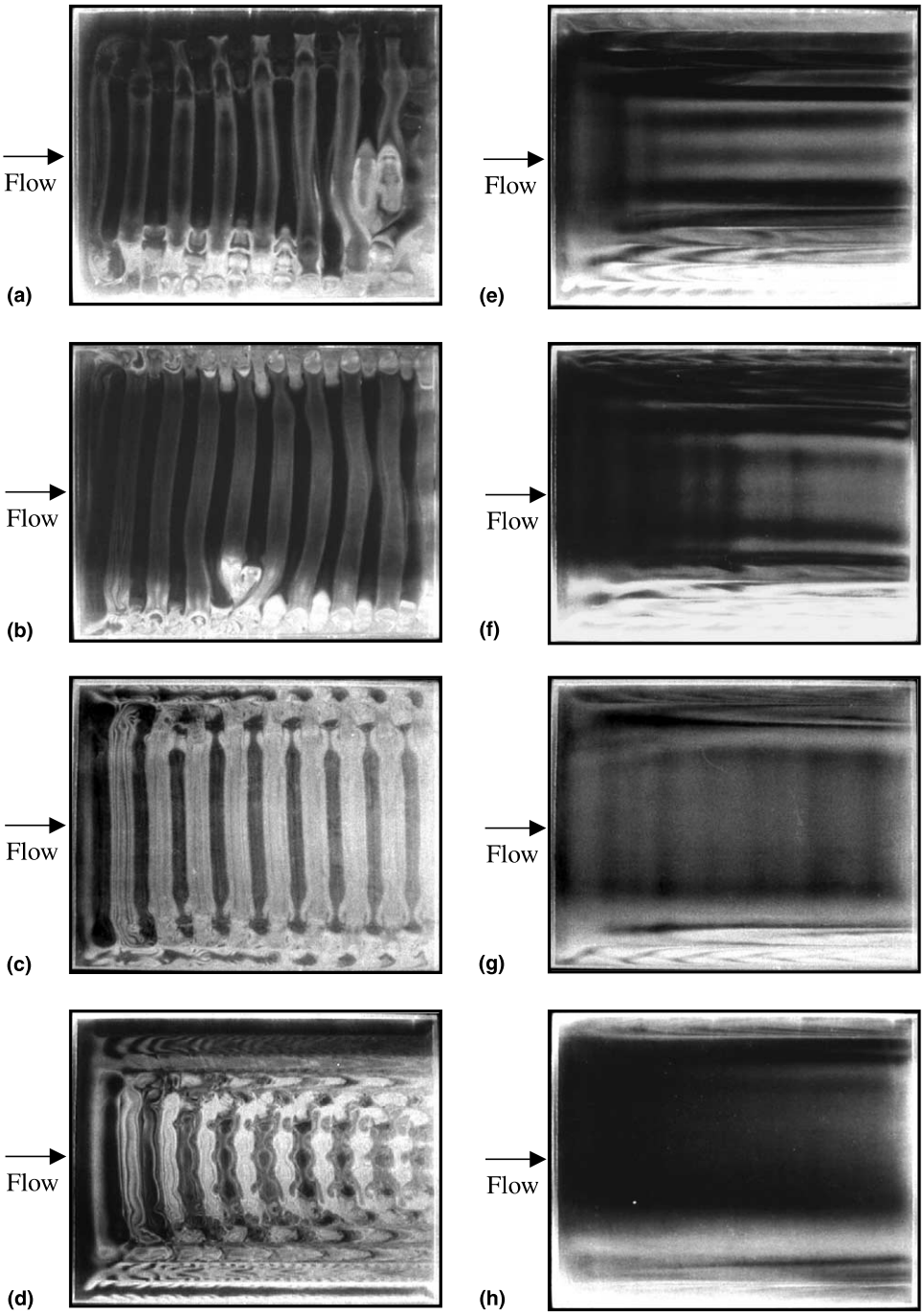


Fig. 2. Top view flow photos at steady or statistical state for $Re = 2.0$ and (a) $Ra = 4000$, (b) $Ra = 3000$, (c) $Ra = 2500$, (d) $Ra = 2000$, (e) $Ra = 1750$, (f) $Ra = 1650$, (g) $Ra = 1500$ and (h) $Ra = 1200$.

more longitudinal rolls are induced near the existing longitudinal rolls (Fig. 2(e)). Hence a steady longitudinal vortex flow prevails in the duct. For a further reduction of $Ra$ to the subcritical level ($Ra = 1650$, 1500 and 1200), only a few longitudinal rolls appear near the duct sides (Figs. 2(f)–(h)). It is of interest to observe that some weakly transverse waves are generated nonperiodically in the core region for the cases with $Ra = 1650$ and 1500.

These transverse waves are pushed by the main forced flow and move downstream. As the buoyancy is further decreased ($Ra = 1200$) these traversing waves disappear and no other secondary flow is induced in the duct core. This appearance of the vortex flow at subcritical buoyancies in the sidewall region is attributed to the fact that near the duct sides the forced main flow is at much lower speed than that in rest of the duct and the cross plane secondary flow can be initiated by the slightly subcritical buoyancy. The vortex flow driven by the subcritical buoyancy was also shown in a numerical simulation to be significant by Ouazzani and Rosenberger [28] in horizontal chemical vapor deposition processes.

Some unfamiliar vortex flow structures are revealed in Fig. 3 by presenting the top view flow photos for various $Ra$ at the lower Reynolds number with $Re = 1.0$. The results for $Re = 1.0$ show that at the high Rayleigh numbers of 4000 and 3000 the buoyancy-to-inertia ratios are so large that highly deformed moving transverse rolls dominate in the duct (Figs. 3(a) and (b)). Obviously, the irregularity in the roll pattern is more severe for the case with a higher buoyancy-to-inertia ratio. The transient temperature measurement indicated that the flow oscillated chaotically in time. The details on the flow regimes observed in this study will be discussed later. It is important to note from Fig. 3(c) that a drastic change in the vortex flow pattern occurs for a reduction of $Ra$ from 3000 to 2500. Specifically, at $Ra = 2500$ the vortex flow is steady and is characterized by a stationary transverse roll at the inlet of the duct, followed immediately by 16 steady longitudinal rolls. All the longitudinal rolls have nearly the same diameter. This unique vortex pattern was not observed in our previous study [6]. However, the presence of this pattern was shown by the stability analysis and numerical and experimental explorations [16,21–24], from various workers as indicated in the last section. The inlet transverse roll is essentially a steady return flow induced by the sudden heating of the flow as it moves from the upstream unheated region into the heated section of the duct. As the buoyancy is lowered further to $Ra = 2000$, the stationary transverse roll merges with the longitudinal rolls adjacent to the duct sides to form a U-roll (Fig. 3(d)). Meanwhile, the beginning portion of the longitudinal rolls near the duct inlet can merge together to form another transverse roll and this transverse roll then merges with the other longitudinal rolls to form a smaller U-roll. Thus, we have another unfamiliar vortex flow which consists of U-rolls and longitudinal rolls. This vortex flow is periodic in time. The U-rolls were reported from a numerical simulation by Spall [29,30] in a lower aspect ratio duct. For even lower $Ra$ of 1750, 1650 and 1500 the stationary transverse rolls at the duct inlet do not merge with the longitudinal rolls. Thus, we have inlet stationary transverse rolls followed by the steady longitudinal rolls (Figs. 3(e)–(g)), similar to that shown in Fig. 3(c) for $Ra = 2500$. But for the lower $Ra(= 1750–1500)$ less longitudinal rolls are induced in the duct and more than one stationary transverse rolls can exist in the duct entry. It is also evidenced from the side view flow photos in Fig. 4 for selected vertical planes that the transverse rolls in the duct inlet are essentially stationary for $Ra = 2500$, 1750 and 1650. But at $Ra = 2000$, the transverse rolls travel a short distance into the test section and merge with the longitudinal rolls in the downstream to form U-rolls (Fig. 4(b)). The results in Fig. 4 also suggest that at a lower $Ra$ the inlet transverse rolls are shorter, smaller and weaker. Besides, transverse rolls also appear near the duct exit for $Ra = 1750$ and 1650 (Figs. 4(c) and (d)). Note that the stationary transverse rolls induced near the duct entry and exit were observed and examined in detail by Visser et al. [31] and Ingle and Mountziaris [32] even at highly subcritical Rayleigh numbers. Besides, these stationary transverse rolls often appear in various metal–organic chemical vapor deposition processes [28,33,34]. At the lowest buoyancy tested here with $Ra = 1200$ nonperiodic traversing transverse waves appear in nearly the entire duct except in the side wall region where a few steady longitudinal rolls prevail (Fig. 3(h)). It should be pointed out here that repeatability tests of the unfamiliar vortex flow patterns examined above have been carried out to ascertain their existence.

### 3.2. Periodical change in vortex flow structures

For the two unfamiliar vortex flow patterns discussed above, the flow consisting of the inlet stationary transverse rolls and downstream longitudinal rolls is steady as the initial transient dies out. On the other hand the flow containing U-rolls is periodic in time. The periodic evolution of the U-rolls is examined in the following. Fig. 5 shows the change in the vortex flow comprising the U-rolls in a typical periodic cycle for the case with $Re = 1.0$ and $Ra = 2000$. The period of the vortex flow $t_p$ is 203 s. Here the dimensional time $t$ denotes certain time instant in the statistical state for that case. Note that at time $t$ a U-roll is formed from the merging of the transverse roll at the duct inlet with the two longitudinal rolls adjacent to the duct sides (Fig. 5(a)). Meanwhile, the upstream ends of the two neighboring longitudinal rolls merge together to form seven slender U-rolls. It is of interest to note that as time proceeds, the transverse portion of the large U-roll slowly moves downstream pushing the slender U-rolls forward and in the mean time a new transverse roll is generated at the duct inlet (Fig. 5(b)). Then, this new transverse roll merges gradually with the two slender U-rolls nearest to the duct sides (Figs. 5 (b) and (c)). As the process continues, more and more moving transverse rolls are induced and six large U-rolls are formed in the duct at time $t + 3/8t_p$ (Fig. 5(d)). However, the junctures between the trans-

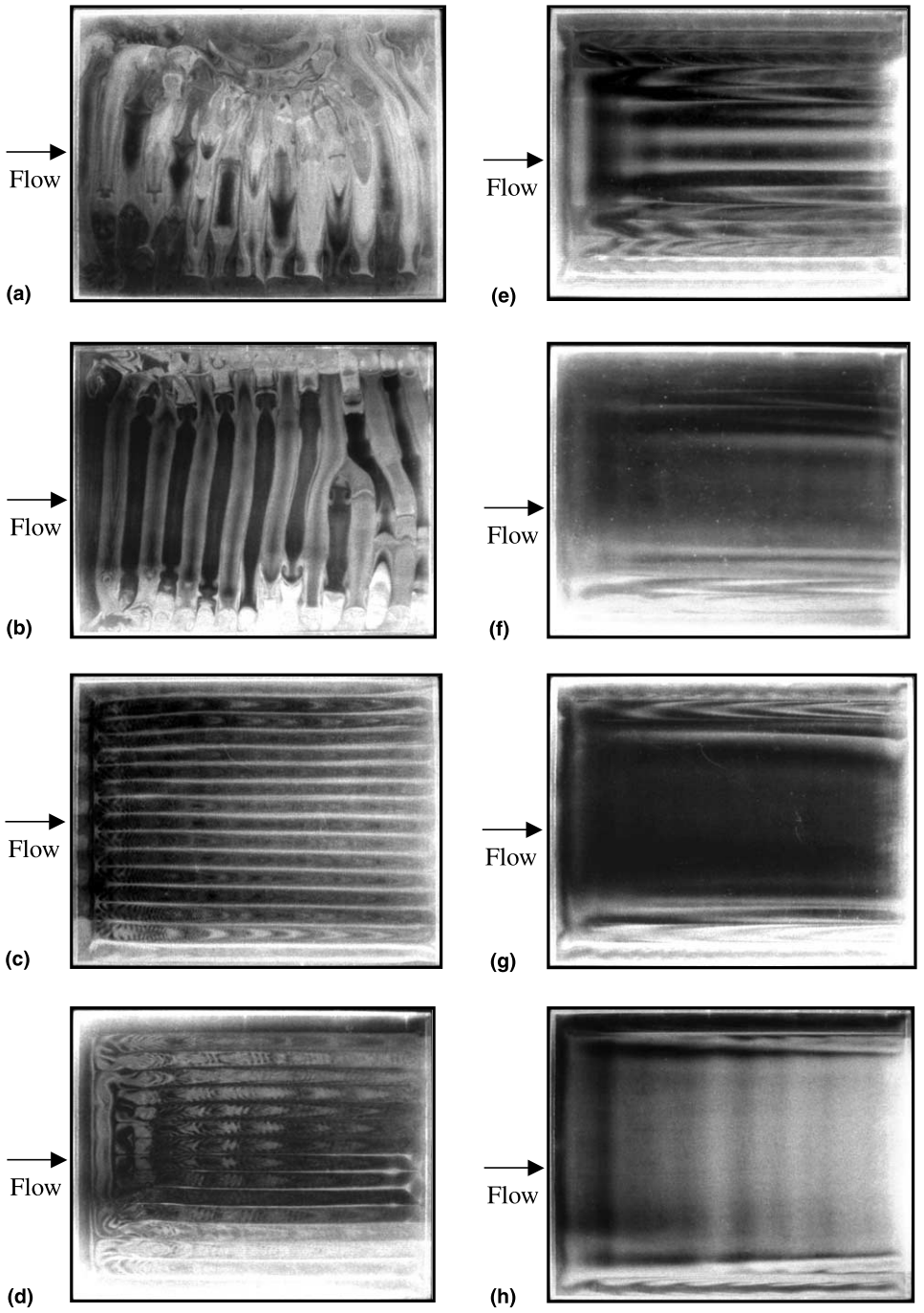


Fig. 3. Top view flow photos at steady or statistical state for $Re = 1.0$ and (a) $Ra = 4000$, (b) $Ra = 3000$, (c) $Ra = 2500$, (d) $Ra = 2000$, (e) $Ra = 1750$, (f) $Ra = 1650$, (g) $Ra = 1500$ and (h) $Ra = 1200$.

verse rolls and the slender U-rolls are somewhat weak and can be broken away to initiate a reverse process for the second half of the periodic cycle for $t \geqslant t + 1/2t_p$. The vortex flow then becomes that shown in Fig. 5(e) including an outermost U-roll, some slender U-rolls, and some short and weak transverse rolls. For a further increase in time the weak transverse rolls in the duct core degenerate and break into cells. Later these cells merge

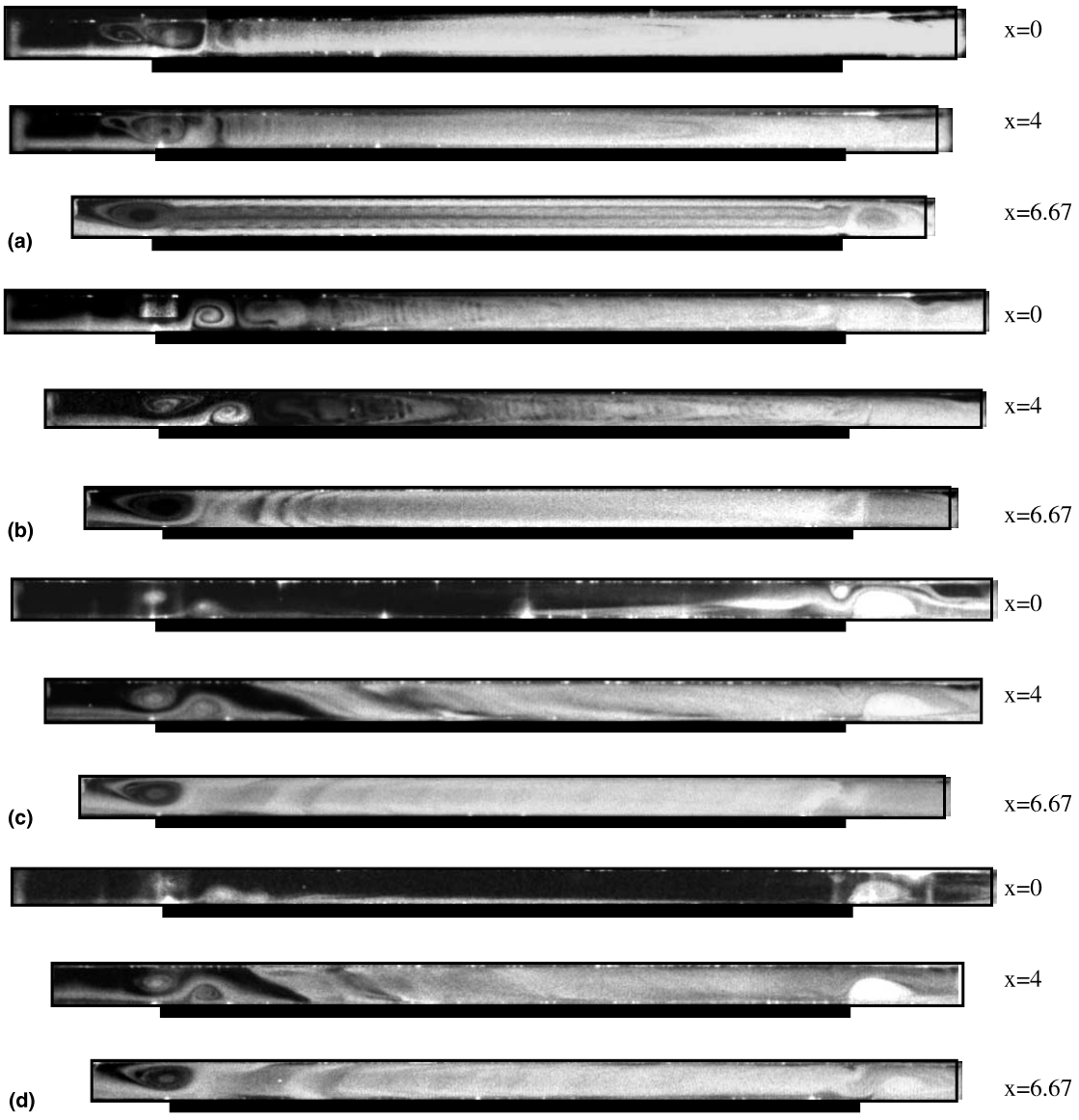


Fig. 4. Side view flow photos at selected vertical planes for $Re = 1.0$ and (a) $Ra = 2500$, (b) $Ra = 2000$, (c) $Ra = 1750$ and (d) $Ra = 1650$.

with the downstream longitudinal rolls (Figs. 5(f) and (g)). At increasing time, most U-rolls gradually disintegrate into longitudinal rolls (Fig. 5(h)). Finally at $t + t_p$, the flow returns to its original state at time $t$ to have only one big U-roll in the duct. To further unravel the structure of the time periodic U-rolls, the corresponding end view flow photos at selected cross sections of the duct are displayed in Fig. 6 for selected time instants. The results suggest that in the entry region of the duct for $z = 1$ and 3.36 the vortices change drastically with time implying the formation and disintegration of the U-rolls in this region. But in the downstream where the longitudinal rolls prevail the change in the vortices is rather mild.

The temporal change of the temperature in the flow is rather significant for the regular and deformed transverse rolls and is shown in Fig. 7 by presenting the time records of the air temperature at selected locations for some cases. The results in Fig. 7(a) for $Re = 2.0$ and $Ra = 2500$ indicate that in the region dominated by the regular transverse rolls the flow is time periodic as our previous study [8]. Moreover, the transverse vortex flow oscillates at the same frequency ($t_p = 11.1$ s) and amplitude in the duct core where the fully developed

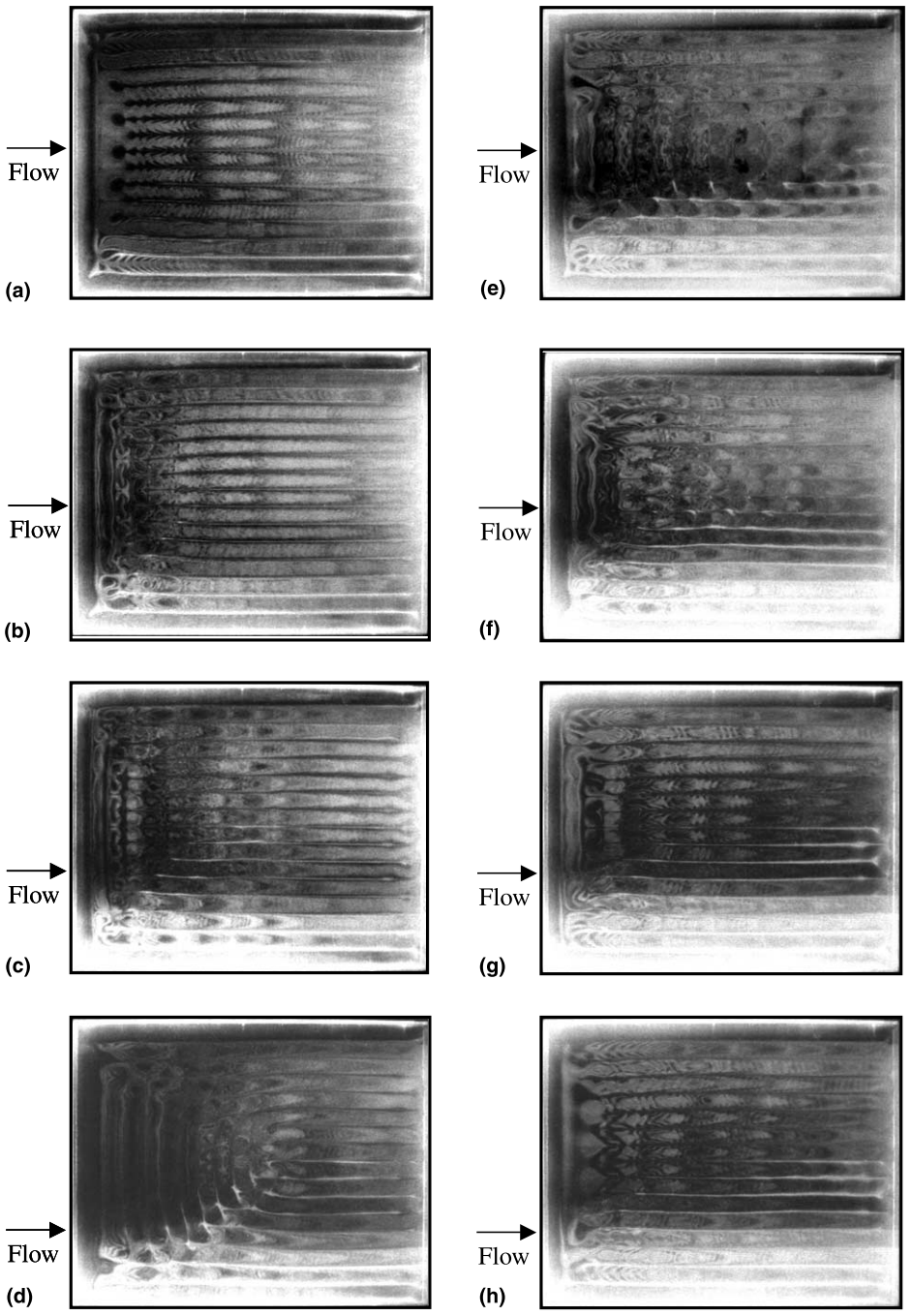


Fig. 5. Top view flow photos for the U-rolls in a typical periodic cycle for $Re = 1.0$ and $Ra = 2000$ at time = (a) $t$, (b) $t + 1/8t_p$, (c) $t + 1/4t_p$, (d) $t + 3/8t_p$, (e) $t + 1/2t_p$, (f) $t + 5/8t_p$, (g) $t + 3/4t_p$ and (h) $t + 7/8t_p$ ($t_p = 203$ s).

transverse rolls prevail. It is of interest to notice that even in the region slightly upstream of the test section the flow oscillates weakly at the same frequency as that in the test section. At higher buoyancy-to-inertia ratios the transverse rolls become larger and can merge together, and the vortex flow becomes somewhat irregular (Figs. 7(b) and (c)). Due to the presence of the irregular vortex rolls in the downstream some irregularity in the temperature oscillation is noted. This irregularity is more severe by further increasing the buoyancy-to-

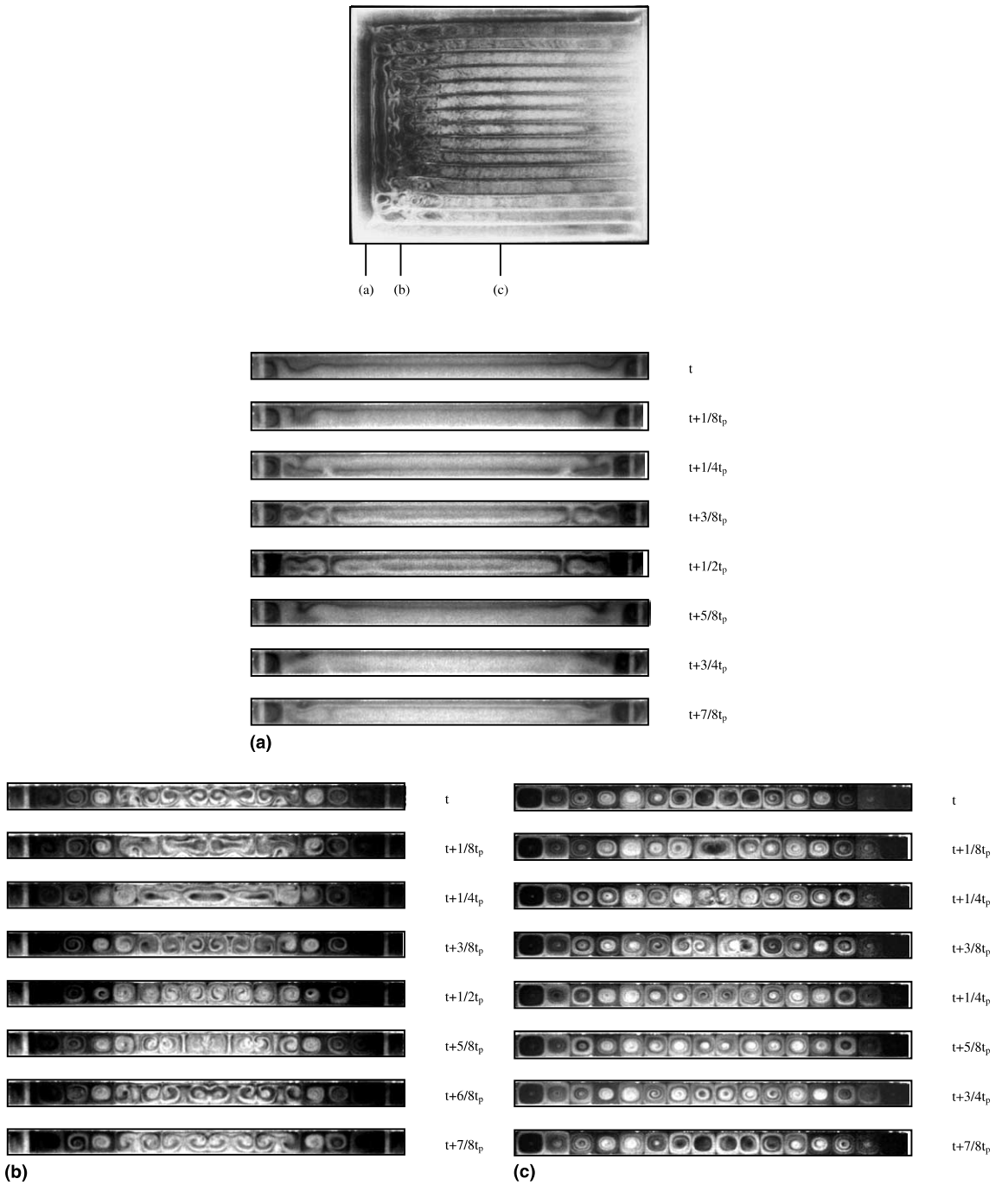


Fig. 6. Top view flow photo for the U-rolls and the corresponding end view flow photos in a typical periodic cycle for $Re = 1.0$ and $Ra = 2000$ at (a) $z = 1$ ($t_p = 38$ s), (b) $z = 3.36$ ($t_p = 203$ s) and (c) $z = 10.09$ ($t_p = 203$ s).

inertia ratio to the case with $Re = 1.0$ and $Ra = 4000$ (Fig. 7(d)).

The time periodic evolution of the vortex flow pattern consisting of the steady longitudinal rolls in the side wall region of the duct, moving transverse rolls in the duct entry and the irregular recirculating cells in the downstream core region of the duct for the case with $Re = 2.0$ and $Ra = 2000$ resembles that for the higher Reynolds number with $Re = 3.0$ discussed in the previous study [8] and the details of this evolution are not

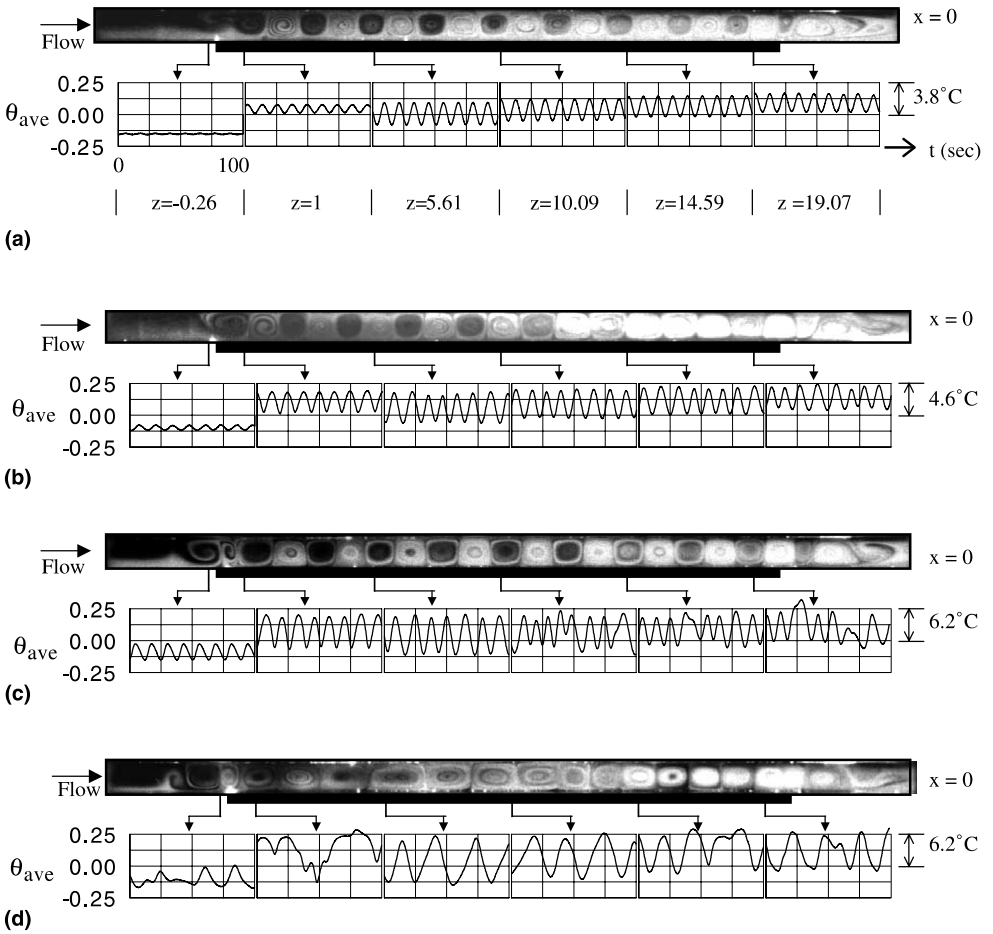


Fig. 7. Side view flow photos at statistical state and the corresponding time records of air temperature at selected locations on the line $y = 1/2$ and $x = 0$ for (a) $Re = 2.0$, $Ra = 2500$ ($t_p = 11.1$ s), (b) $Re = 2.0$, $Ra = 3000$ ($t_p = 11.1$ s), (c) $Re = 2.0$, $Ra = 4000$ ($t_p = 12.1$ s) and (d) $Re = 1.0$, $Ra = 4000$ ($t_p = 21.9$ s).

given here. Moreover, the observed time periodic moving transverse vortex flow at $Re = 2.0$ and $Ra = 2500$ is also similar to that at higher $Re$ [6,8].

### 3.3. Formation of unfamiliar vortex flow patterns

In the mixed convective air flow through a horizontal flat duct heated from below two unfamiliar vortex flow patterns were observed and were examined above for $Ra$ near the critical threshold at $Re = 1.0$. It is important in the fundamental study of heat transfer and fluid dynamics to unveil the processes through which these vortex structures are formed. In the study of the vortex flow formation the experiment is started by setting the Reynolds number at 20.0 and the Rayleigh number at the value for the case to be investigated so that the buoyancy-to-inertia ratio is rather low for a sufficient period of time. Thus, the initial flow ($t < 0$) established in the duct is forced convection dominated. Then, at time $t = 0$ the Reynolds number of the flow is lowered quickly to the level for the specific case to be examined and maintained at this level thereafter for $t > 0$. Note that due to the flow inertia, normally it takes about 10–20 s for the Reynolds number to be reduced to the required level.

The formation of the interesting vortex flow pattern consisting of stationary transverse rolls in the entry region of the duct and stable longitudinal rolls in the downstream is presented in Fig. 8 for $Re = 1.0$ and $Ra = 1750$. Note that this unique vortex pattern is only observed at the lowest Reynolds number tested here at $Re = 1.0$ (Figs. 2 and 3). The results in Fig. 8 indicate that immediately after the reduction of the Reynolds number from 20.0 to 1.0 transverse rolls are repeatedly generated at the duct inlet and longitudinal rolls are successively induced near the duct sides. Note that at this low Reynolds number the transverse rolls travel downstream at a very low speed and they are seriously

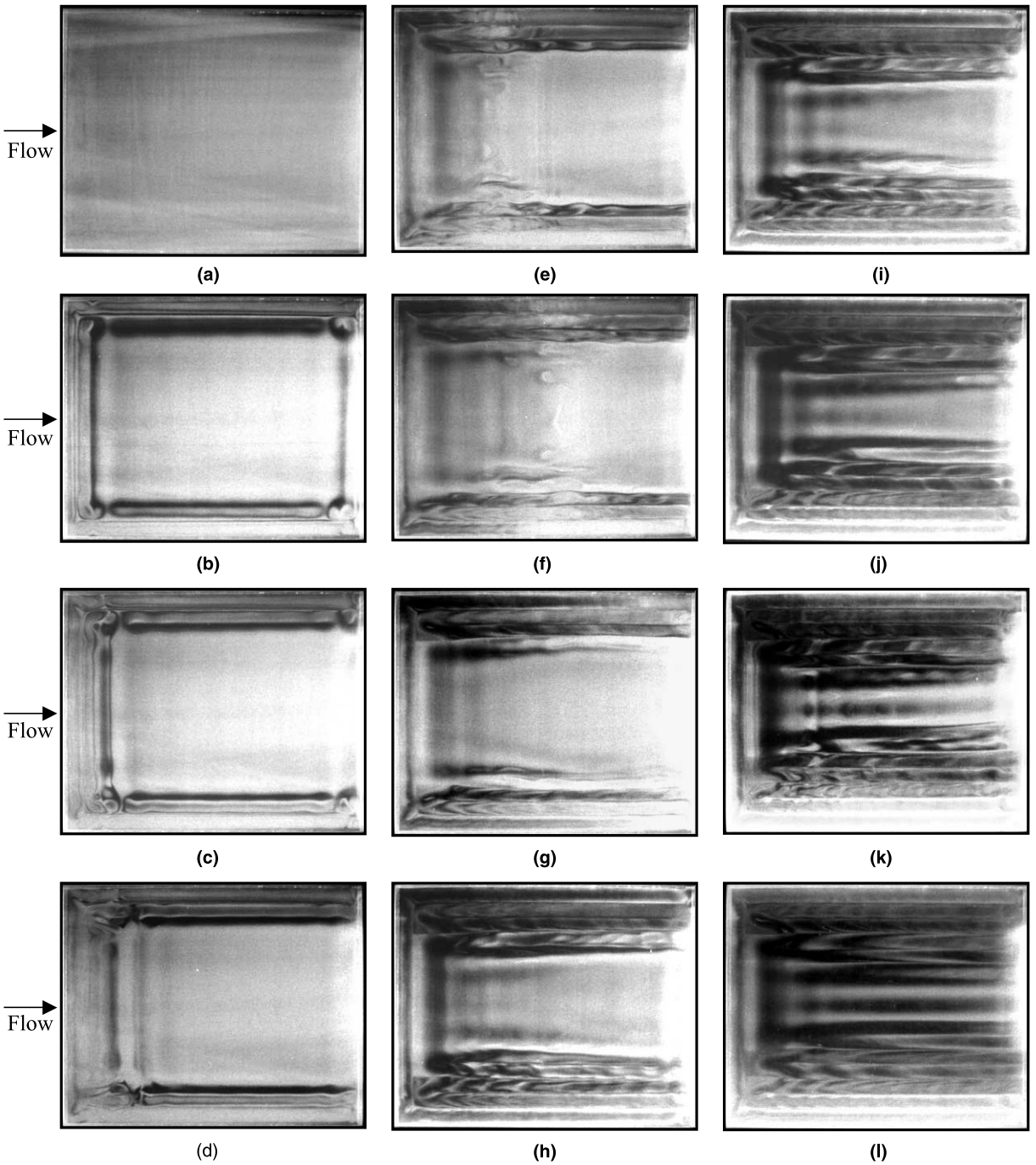


Fig. 8. Top view flow photos showing the formation of stationary transverse rolls in the duct entry and downstream longitudinal rolls by lowering *Re* from 20.0 to 1.0 in 14.2 s for $Ra = 1750$ at time $t =$ (a) 0 s, (b) 19 s, (c) 28 s, (d) 37 s, (e) 77 s, (f) 117 s, (g) 194 s, (h) 346 s, (i) 446 s, (j) 615 s, (k) 807 s and (l) 1079 s.

blocked by the newly induced longitudinal rolls away from the duct sides, as evident from the flow photos in Figs. 8(b) and (c). In fact, the transverse rolls can only travel a short distance before they are completely stopped (Fig. 8(d)). Then the front transverse rolls weaken gradually and later disappear (Fig. 8(e)). The remaining transverse rolls near the duct inlet, however, stay stationary in the duct entry and no new transverse rolls are

generated thereafter (Figs. 8 (f) and (g)). As time proceeds, the stationary transverse rolls get stronger and more longitudinal rolls are induced (Figs. 8(h)–(k)). Finally at $t > 1050$ s, a vortex flow pattern characterized by the inlet stationary transverse rolls along with the downstream stable longitudinal rolls is formed (Fig. 8(l)).

The above vortex flow structure containing the inlet stationary transverse rolls and downstream stable longitudinal rolls also exists at a higher buoyancy for $Re = 1.0$. Fig. 9 shows the formation of such vortex flow driven at $Ra = 2500$. At this higher $Ra$ the transverse and longitudinal rolls are induced in a faster pace following the lowering of the Reynolds number and the rolls are stronger (Fig. 9(b)). It is of interest to note that near the duct exit transverse rolls are also induced at this higher $Ra$. Later, the inlet and exit transverse rolls merge with the longitudinal rolls to form rectangular rolls (Figs. 9(c)–(e)). Meanwhile, the transverse rolls in the duct entry slowly move downstream and hence push the rectangular rolls forward. Besides, new transverse roll is repeatedly generated at the duct inlet. Note that the downstream end of the rectangular rolls leaves the duct at a certain time instant and we observe slightly deformed U-rolls in the duct (Fig. 9(f)). As time proceeds, the transverse rolls weaken and the U-rolls become more deformed (Fig. 9(g)). Moreover, the outer U-rolls near the duct inlet and duct sides split into slightly deformed transverse and longitudinal rolls. Then, the deformed transverse rolls disintegrate into recirculating cells. These cells later merge together to form short longitudinal rolls (Figs. 9 (h) and (i)). The longitudinal rolls gradually strengthen up and extend towards the duct exit to merge with the U-rolls. This process continues and more and more longitudinal rolls are formed (Figs. 9(i)–(k)). But only one transverse roll exists at the duct inlet. The deformed longitudinal rolls take certain period of time to become straight, and finally at $t > 510$ s a vortex flow pattern comprising of an inlet stationary roll and downstream stable longitudinal rolls is reached.

In the vortex flow evolution leading to the U-rolls, moving transverse rolls are also repeatedly generated in the duct entry and longitudinal rolls are induced near the duct sides in the initial transient (Figs. 10(b) and (c)). Later, the transverse and longitudinal rolls merge together to form a few U-rolls (Figs. 10(d) and (e)). These U-rolls are distorted to a certain degree and the roll distortion increases with time. Note that at $t = 149$ s the rolls become rather irregular. But a stationary, outermost U-roll with its legs along the duct sides is clearly seen (Fig. 10(f)). Besides, a regular transverse roll is seen near the duct inlet. Then, it is of interest to observe the appearance of short longitudinal rolls in the entry half of the duct (Fig. 10(g)). As the process continues, these longitudinal rolls grow slowly in the downstream direction. Meanwhile, the transverse roll and longitudinal rolls merge together to form a U-roll (Fig. 10(h)). Then, the transverse portion of the U-rolls move slowly downstream and a new transverse roll is generated at the duct inlet. This newly formed transverse roll and the transverse portions of the U-rolls merge with the longitudinal rolls to form U-rolls. In this process one more U-roll appears (Figs. 10 (i) and (j)). Note that the U-rolls away from the duct entry are rather weak and later disintegrate into cells (Figs. 10(i) and (j)). These cells then merge together to form longitudinal rolls (Fig. 10(k)). Note that in the region between the U-rolls there appear several longitudinal rolls. Finally, at $t > 680$ s a vortex flow pattern characterized by a few U-rolls with several longitudinal rolls contained in the space between the U-rolls is formed.

### 3.4. Flow regime map

Based on the present data and the data obtained in the previous study [8], various vortex flow patterns induced in the low Reynolds number mixed convective air flow in a bottom heated horizontal flat duct are summarized in a flow regime map given in Fig. 11. Also indicated in the map is the condition around which the vortex flows consisting of stable longitudinal rolls near the duct sides and nonperiodic traversing transverse waves in the duct core. This condition can be roughly represented by the equation

$$Ra_c^{NW} \approx 1750 - 540/Re^2. \quad (1)$$

Moreover, the boundary between the regular transverse vortex flow and the mixed vortex flow which is characterized by the stable longitudinal rolls near the duct sides and the time periodic moving transverse rolls in the duct core can be approximately expressed as

$$Ra_c^{T} \approx 2200 + 1.7\,Re^4. \quad (2)$$

Finally, the transition between the regular transverse rolls and deformed transverse rolls occurs at

$$Ra_c^{IT} \approx 2700 + 0.2\,Re^9. \quad (3)$$

For comparison purpose the vortex flow patterns for the limiting case of the natural convective flow in the test section, i. e., for $Re = 0$, are also indicated in the map. In the natural convection test the inlet and exit of the test section are completely closed by placing plexiglass plates at these locations. Note that for $Re = 0$ the entire test section, which is essentially a horizontal rectangular enclosure, is filled with the stationary transverse rolls for $2000 \leqslant Ra \leqslant 3000$. The rolls are parallel with the short sides of the enclosure [26]. For $Ra = 4000$ deformed transverse rolls prevail. But at the lower buoyancy for $Ra \leqslant 1750$ rectangular rolls dominate in the enclosure. In broad sense these vortex

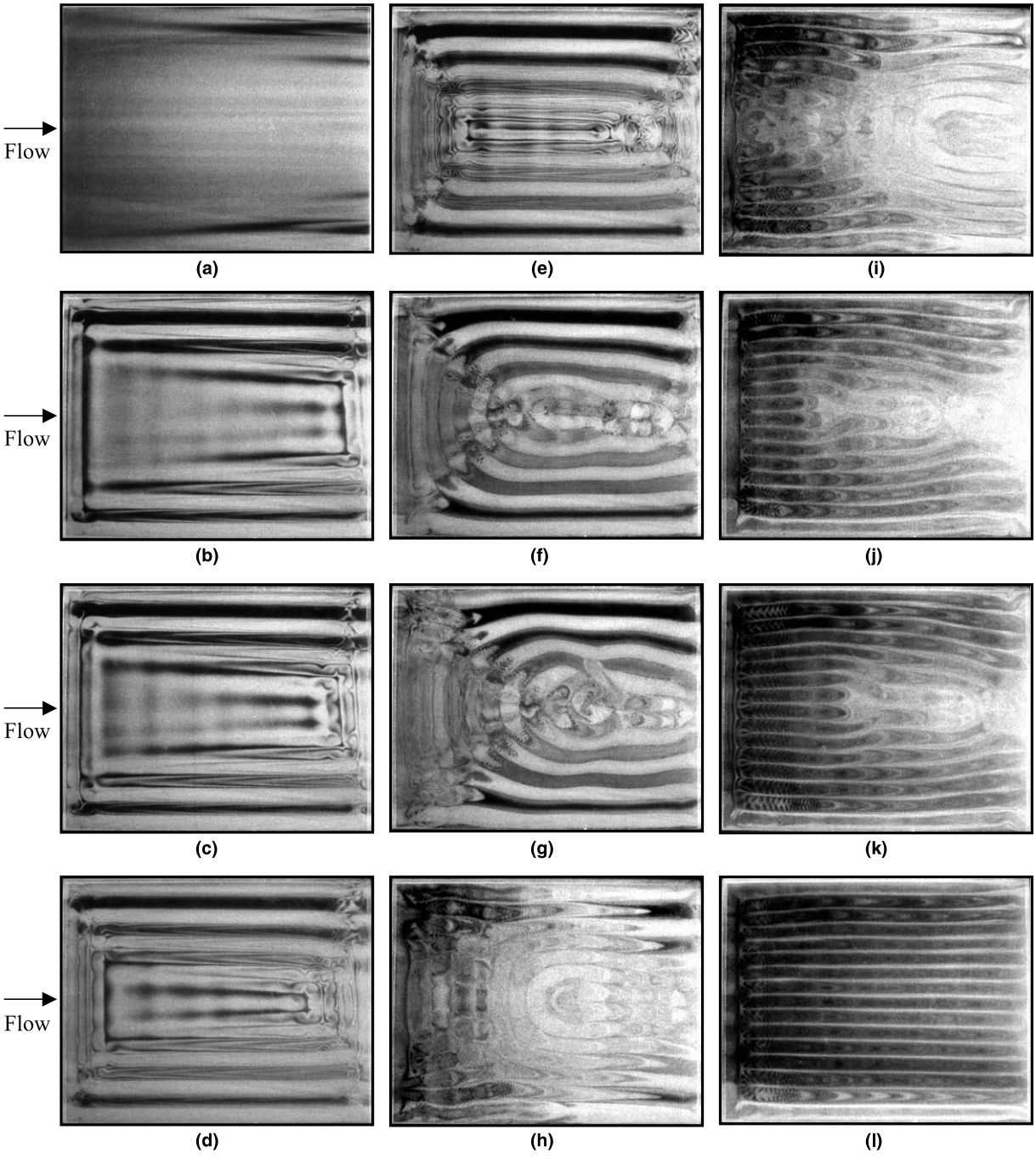


Fig. 9. Top view flow photos showing the formation of stationary transverse rolls in the duct entry and downstream longitudinal rolls by lowering $Re$ from 20.0 to 1.0 in 14.5 s for $Ra = 2500$ at time $t =$ (a) 0 s, (b) 6 s, (c) 8 s, (d) 14 s, (e) 20 s, (f) 39 s, (g) 58 s, (h) 152 s, (i) 178 s, (j) 247 s, (k) 296 s and (l) 519 s.

flow patterns for $Re = 0$ are somewhat related to those at $Re = 1.0$. The details on these natural convective vortex flow patterns were examined in an earlier study [35].

## 4. Concluding remarks

A study combining experimental flow visualization and temperature measurement has been carried out here

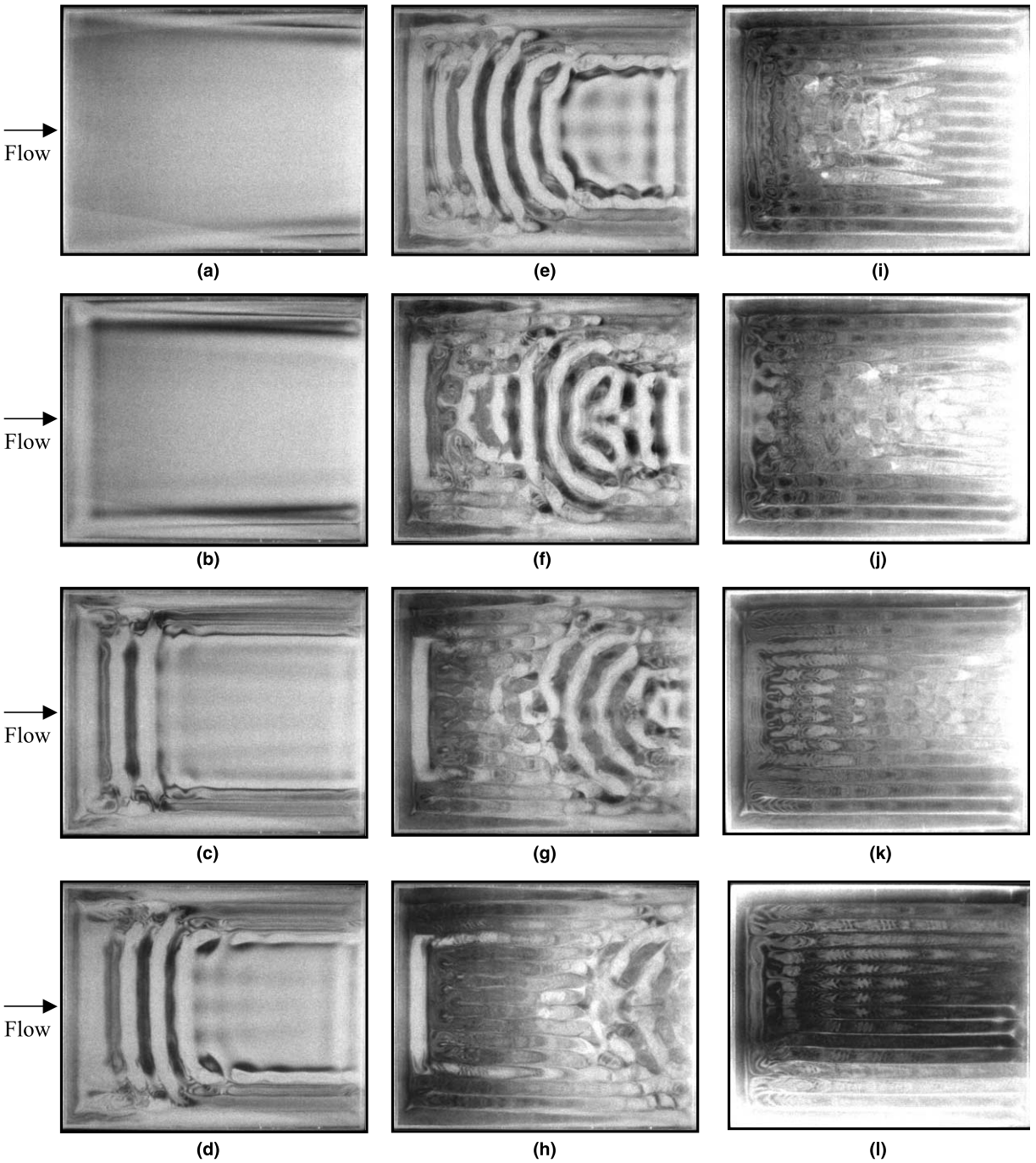


Fig. 10. Top view flow photos showing the formation of U-rolls by lowering *Re* from 20.0 to 1.0 in 14.8 s for $Ra = 2000$ at time $t =$ (a) 0 s, (b) 6 s, (c) 28 s, (d) 43 s, (e) 69 s, (f) 149 s, (g) 201 s, (h) 275 s, (i) 496 s, (j) 612 s, (k) 620 s and (l) 716 s.

to explore the buoyancy driven vortex flow structures in a mixed convective air flow in a bottom heated horizontal flat duct at a very low Reynolds number approaching the natural convection limit for the Rayleigh number around the critical level for the onset of convection, including the subcritical and supercritical states. Results from the present study have revealed some interesting but unfamiliar vortex flow structures. In particular, we identify two unfamiliar structures, namely, the vortex flow comprising stationary transverse rolls in

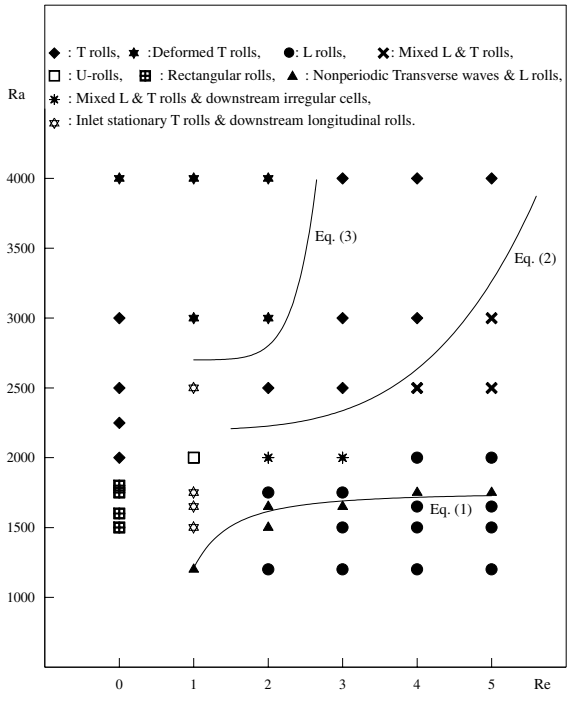


Fig. 11. Flow regime map for different vortex flow patterns observed in flow visualization.

the duct entry and stable longitudinal rolls in the downstream, and the vortex flow containing U-rolls.

The formation processes leading to these two vortex flow patterns observed in the present experiment are also examined in detail. The results disclose many complicate processes during the vortex flow formation, including the generation of the longitudinal and transverse rolls, merging of longitudinal and transverse rolls to form U-rolls, splitting of rolls into cells and the reverse process of integrating cells into rolls. Besides, a flow regime map is given to delineate various vortex flow patterns in the limiting low Reynolds number mixed convective flow.

## Acknowledgements

The financial support of this study by the engineering division of National Science Council of Taiwan, ROC through the contract NSC83 0404 E009 054 is greatly appreciated.

## References

[1] K.C. Chiu, F. Rosenberger, Mixed convection between horizontal plates – I. Entrance effects, Int. J. Heat Mass Transfer 30 (8) (1987) 1645–1654.

[2] K.C. Chiu, J. Ouazzani, F. Rosenberger, Mixed convection between horizontal plates – II. Fully developed flow, Int. J. Heat Mass Transfer 30 (8) (1987) 1655–1662.

[3] M.T. Ouazzani, J.P. Caltagirone, G. Meyer et A. Mojtabi, Etude numérique et expérimentale de la convection mixte entre deux plans horizontaux á températures différences, Int. J. Heat Mass Transfer 32 (2) (1989) 261–269.

[4] M.T. Ouazzani, J.K. Platten et A. Mojtabi, Etude expérimentale de la convection mixte entre deux plans horizontaux á températures différences – II, Int. J. Heat Mass Transfer 33 (7) (1990) 1417–1427.

[5] M.T. Ouazzani, J.K. Platten et A. Mojtabi, Intermittent patterns in mixed convection, Appl. Sci. Res. 51 (1993) 677–685.

[6] M.Y. Chang, T.F. Lin, Vortex flow pattern selection and temporal – spatial structures of transverse and mixed vortex rolls in mixed convection of air in a horizontal flat duct, Phys. Rev. E 54 (1996) 5146–5160.

[7] C.H. Yu, M.Y. Chang, T.F. Lin, Structure of moving transverse and mixed rolls in mixed convection of air in a horizontal plane channel, Int. J. Heat Mass Transfer 40 (2) (1997) 333–346.

[8] J.T. Lir, M.Y. Chang, T.F. Lin, Vortex flow patterns near critical state for onset of convection in air flow through a bottom heated horizontal flat duct, Int. J. Heat Mass Transfer 44 (4) (2001) 705–719.

[9] M.L. Hitchman, K.F. Jensen, Chemical Vapor Deposition – Principles and Applications, Academic Press, San Diego, 1993 (Chapter 2).

[10] M. Akiyama, G.J. Hwang, K.C. Cheng, Experiments on the onset of longitudinal vortices in laminar forced convection between horizontal plates, J. Heat Transfer 93 (1971) 335–341.

[11] S. Ostrach, Y. Kamotani, Heat transfer augmentation in laminar fully developed flow by means of heating from below, J. Heat Transfer 97 (1975) 220–225.

[12] Y. Kamotani, S. Ostrach, Effect of thermal instability on thermally developing channel flow, J. Heat Transfer 98 (1976) 62–66.

[13] G.J. Hwang, K.C. Cheng, Convective instability in the thermal entrance region of a horizontal parallel-plate channel heated from below, J. Heat Transfer 95 (1973) 72–77.

[14] H.K. Moffat, K.F. Jensen, Complex flow phenomena in MOCVD reactors, J. Crystal Growth 77 (1986) 108–119.

[15] H.K. Moffat, K.F. Jensen, Three-dimensional flow effects in silicon CVD in horzontal reactors, J. Electro Chem. Soc. 135 (1988) 459–471.

[16] H.W. Müller, M. Lücke, M. Kamps, Transversal convection patterns in horizontal shear flow, Phys. Rev. A 45 (1992) 3714–3725.

[17] H.W. Müller, M. Tveitereid, S. Trainoff, Rayleigh–Bénard problem with imposed weak through-flow: two coupled Ginzburg–Landau equations, Phys. Rev. E 48 (1993) 263.

[18] M. Tveitereid, H.W. Müller, Pattern selection at the onset of Rayleigh–Bénard convection in a horizontal shear flow, Phys Rev. E 50 (1994) 1219.

[19] J.M. Luijkx, J.K. Platten, On the existence of thermoconvective rolls transverse to a superimposed mean Poiseuille flow, Int. J. Heat Mass Transfer 24 (7) (1981) 1287–1291.

[20] J.K. Platten, J.C. Legros, Convection in Liquids, Springer, Berlin, 1984 (Chapters 6 and 7).
[21] K.C. Cheng, R.S. Wu, Axial heat conduction effects on thermal instability of horizontal plane Poiseuille flows heated from below, J. Heat Transfer 98 (1976) 564–569.
[22] E. Schröder, K. Bühler, Three-dimensional convection in rectangular domains with horizontal throughflow, Int. J. Heat Mass Transfer 38 (7) (1995) 1249–1259.
[23] D. Roth, P. Büchel, M. Lücke, H.W. Müller, M. Kamps, R. Schmitz, Influence of boundaries on pattern selection in through-flow, Physica D 97 (1996) 253–263.
[24] X. Nicolas, A. Mojtabi, Two-dimensional numerical analysis of the Poiseuille–Bénard flow in a rectangular channel heated from below, Phys. Fluids 9 (2) (1997) 337–348.
[25] X. Nicolas, J.M. Luijkx, J.K. Platten, Linear stability of mixed convection flows in horizontal rectangular channels of finite transversal extension heated from below, Int. J. Heat Mass Transfer 43 (4) (2000) 589–610.
[26] E.L. Koschmieder, Bénard Cells and Taylor Vortices, Cambridge University Press, Cambridge, 1993 (Chapter 5).
[27] S.J. Kline, F.A. McClintock, Describing uncertainties in single-sample experiments, Mech. Eng. 75 (1953) 3–12.
[28] J. Ouazzani, F. Rosenberger, Three-dimensional modelling of horizontal chemical vapor deposition I. MOCVD at atmospheric pressure, J. Crystal Growth 100 (1990) 545–576.
[29] R.E. Spall, Unsteady mixed convection in horizontal ducts with applications to chemical vapor deposition processes, Int. Comm. Heat Mass Transfer 23 (1) (1996) 115–122.
[30] R.E. Spall, Observations of spanwise symmetry breaking for unsteady mixed convection in horizontal ducts, J. Heat Transfer 118 (1996) 885–888.
[31] E.P. Visser, C.R. Kleijn, C.A.M. Govers, C.J. Hoogendoorn, L.J. Giling, Return flows in horizontal MOCVD reactors studied with the use of $TiO_2$ particle injection and numerical calculations, J. Crystal Growth 94 (1989) 929–946.
[32] N.K. Ingle, T.J. Mountziaris, The onset of transverse recirculations during flow of gases in horizontal ducts with differentially heated lower walls, J. Fluid Mech. 277 (1994) 249–269.
[33] C.R. Kleijn, C.J. Hoogendoorn, A study of 2-D and 3-D transport phenomena in horizontal chemical vapor deposition reactors, Chem. Eng. Sci. 46 (1) (1991) 321–334.
[34] K.W. Park, H.Y. Pak, Characteristics of three-dimensional flow, heat, and mass transfer in a chemical vapor deposition reactor, Numer. Heat Transfer, Part A 37 (2000) 407–423.
[35] J.T. Lir, T.F. Lin, Visualization of roll patterns in Rayleigh–Bénard convection of air in a rectangular shallow cavity, Int. J. Heat Mass Transfer 44 (15) (2001) 2889–2902.